

## Measurement of the $B_s^0$ lifetime

OPAL Collaboration

P D Acton<sup>y</sup>, R Akers<sup>p</sup>, G Alexander<sup>w</sup>, J Allison<sup>p</sup>, K J Anderson<sup>t</sup>, S Arce<sup>l</sup>, A Astbury<sup>ab</sup>,  
D Axen<sup>ac</sup>, G Azuelos<sup>r,1</sup>, J T M Baines<sup>p</sup>, A H Ball<sup>q</sup>, J Banks<sup>p</sup>, R J Barlow<sup>p</sup>, S Barnett<sup>p</sup>,  
R Bartoldus<sup>c</sup>, J R Batley<sup>e</sup>, G Beaudoin<sup>r</sup>, A Beck<sup>w</sup>, G A Beck<sup>m</sup>, J Becker<sup>j</sup>, C Beeston<sup>p</sup>,  
T Behnke<sup>aa</sup>, K W Bell<sup>t</sup>, G Bella<sup>w</sup>, P Bentkowski<sup>r</sup>, P Berlich<sup>j</sup>, S Bethke<sup>k</sup>, O Biebel<sup>c</sup>,  
I J Bloodworth<sup>a</sup>, P Bock<sup>k</sup>, B Boden<sup>c</sup>, H M Bosch<sup>k</sup>, M Boutemeur<sup>r</sup>, H Breuker<sup>h</sup>,  
P Bright-Thomas<sup>y</sup>, R M Brown<sup>t</sup>, A Buys<sup>h</sup>, H J Burckhart<sup>h</sup>, C Burgard<sup>aa</sup>, P Capiluppi<sup>b</sup>,  
R K Carnegie<sup>f</sup>, A A Carter<sup>m</sup>, J R Carter<sup>e</sup>, C Y Chang<sup>q</sup>, D G Charlton<sup>h</sup>, S L Chu<sup>d</sup>,  
P E L Clarke<sup>o</sup>, J C Clayton<sup>a</sup>, I Cohen<sup>w</sup>, J E Conboy<sup>o</sup>, M Cooper<sup>v</sup>, M Coupland<sup>n</sup>,  
M Cuffiani<sup>b</sup>, S Dado<sup>v</sup>, G M Dallavalle<sup>b</sup>, S De Jong<sup>m</sup>, L A del Pozo<sup>e</sup>, H Deng<sup>q</sup>,  
A Dieckmann<sup>k</sup>, M Dittmar<sup>d</sup>, M S Dixit<sup>g</sup>, E do Couto e Silva<sup>l</sup>, J E Duboscq<sup>h</sup>, E Duchovni<sup>z</sup>,  
G Duckeck<sup>k</sup>, I P Duerdoth<sup>p</sup>, D J P Dumas<sup>f</sup>, P A Elcombe<sup>e</sup>, P G Estabrooks<sup>f</sup>, E Etzion<sup>w</sup>,  
H G Evans<sup>t</sup>, F Fabbri<sup>b</sup>, B Fabbro<sup>u</sup>, M Fierro<sup>b</sup>, M Fincke-Keeler<sup>ab</sup>, H M Fischer<sup>c</sup>,  
D G Fong<sup>q</sup>, M Foucher<sup>q</sup>, A Gaidot<sup>u</sup>, J W Gary<sup>d</sup>, J Gascon<sup>r</sup>, N I Geddes<sup>t</sup>,  
C Geich-Gimbel<sup>c</sup>, S W Gensler<sup>t</sup>, F X Gentit<sup>u</sup>, G Giacomelli<sup>b</sup>, R Giacomelli<sup>b</sup>, V Gibson<sup>e</sup>,  
W R Gibson<sup>m</sup>, J D Gillies<sup>t</sup>, J Goldberg<sup>v</sup>, D M Gingrich<sup>ad,1</sup>, M J Goodrick<sup>e</sup>, W Gorn<sup>d</sup>,  
C Grandi<sup>b</sup>, F C Grant<sup>e</sup>, J Hagemann<sup>aa</sup>, G G Hanson<sup>l</sup>, M Hansroul<sup>h</sup>, C K Hargrove<sup>g</sup>,  
P F Harrison<sup>m</sup>, J Hart<sup>h</sup>, P M Hattersley<sup>a</sup>, M Hauschild<sup>h</sup>, C M Hawkes<sup>h</sup>, E Heflin<sup>d</sup>,  
R J Hemingway<sup>f</sup>, G Herten<sup>j</sup>, R D Heuer<sup>h</sup>, J C Hill<sup>e</sup>, S J Hillier<sup>h</sup>, T Hulse<sup>j</sup>, D A Hinshaw<sup>r</sup>,  
J D Hobbs<sup>h</sup>, P R Hobson<sup>y</sup>, D Hochman<sup>z</sup>, R J Homer<sup>a</sup>, A K Honma<sup>ab,1</sup>, R E Hughes-  
Jones<sup>p</sup>, R Humbert<sup>j</sup>, P Igo-Kemenes<sup>k</sup>, H Ihssen<sup>k</sup>, D C Imrie<sup>y</sup>, A C Janissen<sup>f</sup>, A Jawahery<sup>q</sup>,  
P W Jeffreys<sup>t</sup>, H Jeremie<sup>r</sup>, M Jimack<sup>a</sup>, M Jones<sup>ac</sup>, R W L Jones<sup>h</sup>, P Jovanovic<sup>a</sup>, C Jui<sup>d</sup>,  
D Karlen<sup>f</sup>, K Kawagoe<sup>x</sup>, T Kawamoto<sup>x</sup>, R K Keeler<sup>ab</sup>, R G Kellogg<sup>q</sup>, B W Kennedy<sup>o</sup>,  
S Kluth<sup>e</sup>, T Kobayashi<sup>x</sup>, D S Koetke<sup>h</sup>, T P Kokott<sup>c</sup>, S Komamiya<sup>x</sup>, L Kopke<sup>h</sup>, J F Kral<sup>h</sup>,  
R Kowalewski<sup>f</sup>, J von Krogh<sup>k</sup>, J Kroll<sup>t</sup>, M Kuwano<sup>x</sup>, P Kyberd<sup>m</sup>, G D Lafferty<sup>p</sup>,  
H Lafoux<sup>u</sup>, R Lahmann<sup>q</sup>, F Lamarche<sup>r</sup>, J G Layter<sup>d</sup>, P Leblanc<sup>r</sup>, A M Lee<sup>ae</sup>, M H Lehto<sup>o</sup>,  
D Lellouch<sup>z</sup>, C Leroy<sup>r</sup>, J Letts<sup>d</sup>, S Levegrun<sup>c</sup>, L Levinson<sup>z</sup>, S L Lloyd<sup>m</sup>, F K Loebinger<sup>p</sup>,  
J M Lorah<sup>q</sup>, B Lorazo<sup>r</sup>, M J Losty<sup>g</sup>, X C Lou<sup>l</sup>, J Ludwig<sup>j</sup>, A Luig<sup>j</sup>, M Mannelli<sup>h</sup>,  
S Marcellini<sup>b</sup>, C Markus<sup>c</sup>, A J Martin<sup>m</sup>, J P Martin<sup>r</sup>, T Mashimo<sup>x</sup>, P Mattig<sup>c</sup>, U Maur<sup>c</sup>,  
J McKenna<sup>ab</sup>, T J McMahon<sup>a</sup>, J R McNutt<sup>y</sup>, F Meijers<sup>h</sup>, D Menszner<sup>k</sup>, F S Merritt<sup>t</sup>,  
H Mes<sup>g</sup>, A Micheli<sup>h</sup>, R P Middleton<sup>t</sup>, G Mikenberg<sup>z</sup>, J Mildener<sup>f</sup>, D J Miller<sup>o</sup>,  
R Mir<sup>l</sup>, W Mohr<sup>j</sup>, C Moisan<sup>r</sup>, A Montanari<sup>b</sup>, T Mori<sup>x</sup>, M Moru<sup>x</sup>, U Muller<sup>c</sup>, B Nellen<sup>c</sup>,  
H H Nguyen<sup>t</sup>, S W O'Neale<sup>a</sup>, F G Oakham<sup>g</sup>, F Odorici<sup>b</sup>, H O Ogren<sup>l</sup>, C J Oram<sup>ab,1</sup>,  
M J Oreglia<sup>t</sup>, S Orito<sup>x</sup>, J P Pansart<sup>u</sup>, B Panzer-Steindel<sup>h</sup>, P Paschivici<sup>z</sup>, G N Patrick<sup>t</sup>,  
N Paz-Jaoshvili<sup>w</sup>, M J Pearce<sup>a</sup>, P Pfister<sup>j</sup>, J E Pilcher<sup>t</sup>, J Pinfold<sup>ad</sup>, D Pitman<sup>ab</sup>,  
D E Plane<sup>h</sup>, P Poffenberger<sup>ab</sup>, B Poli<sup>b</sup>, A Pouladdej<sup>f</sup>, T W Pritchard<sup>m</sup>, H Przywiecniak<sup>r</sup>,  
G Quast<sup>aa</sup>, M W Redmond<sup>h</sup>, D L Rees<sup>h</sup>, G E Richards<sup>p</sup>, S A Robins<sup>m</sup>, D Robinson<sup>h</sup>,  
A Rollnik<sup>c</sup>, J M Roney<sup>ab,2</sup>, E Ros<sup>h</sup>, S Rossberg<sup>j</sup>, A M Rossi<sup>b</sup>, M Rosvick<sup>ab</sup>,  
P Routenburg<sup>f</sup>, K Runge<sup>j</sup>, O Runolfsson<sup>h</sup>, D R Rust<sup>l</sup>, M Sasaki<sup>x</sup>, C Sbarra<sup>b</sup>, A D Schaile<sup>j</sup>,  
O Schaile<sup>j</sup>, W Schappert<sup>f</sup>, P Scharff-Hansen<sup>h</sup>, P Schenk<sup>d</sup>, B Schmitt<sup>c</sup>, H von der Schmitt<sup>k</sup>,

M Schroder<sup>ℓ</sup>, C Schwick<sup>aa</sup>, J Schwiening<sup>c</sup>, W G Scott<sup>l</sup>, M Settles<sup>ℓ</sup>, T G Shears<sup>e</sup>, B C Shen<sup>d</sup>, C H Shepherd-Themistocleous<sup>g</sup>, P Sherwood<sup>o</sup>, G P Siroli<sup>b</sup>, A Skillman<sup>p</sup>, A Skuja<sup>q</sup>, A M Smith<sup>h</sup>, T J Smith<sup>ab</sup>, G A Snow<sup>q</sup>, R Sobie<sup>ab,2</sup>, R W Springer<sup>q</sup>, M Sproston<sup>t</sup>, A Stahl<sup>c</sup>, C Stegmann<sup>j</sup>, K Stephens<sup>p</sup>, J Steuerer<sup>ab</sup>, R Strohmmer<sup>k</sup>, D Strom<sup>s</sup>, H Takeda<sup>x</sup>, T Takeshita<sup>x,3</sup>, S Tarem<sup>z</sup>, M Tecchio<sup>l</sup>, P Teixeira-Dias<sup>k</sup>, N Tesch<sup>c</sup>, M A Thomson<sup>o</sup>, E Torrente-Lujan<sup>v</sup>, S Towers<sup>ab</sup>, G Transtomer<sup>y</sup>, N J Tresilian<sup>p</sup>, T Tsukamoto<sup>x</sup>, M F Turner<sup>h</sup>, D Van den plas<sup>r</sup>, R Van Kooten<sup>aa</sup>, G J VanDalen<sup>d</sup>, G Vasseur<sup>u</sup>, C J Virtue<sup>g</sup>, A Wagner<sup>aa</sup>, D L Wagner<sup>l</sup>, C Wahl<sup>j</sup>, C P Ward<sup>e</sup>, D R Ward<sup>e</sup>, P M Watkins<sup>a</sup>, A T Watson<sup>a</sup>, N K Watson<sup>h</sup>, M Weber<sup>k</sup>, P Weber<sup>f</sup>, P S Wells<sup>h</sup>, N Vermes<sup>c</sup>, M A Whalley<sup>a</sup>, B Wilkens<sup>j</sup>, G W Wilson<sup>d</sup>, J A Wilson<sup>a</sup>, V-H Winterer<sup>j</sup>, T Wlodek<sup>z</sup>, G Wolf<sup>z</sup>, S Wotton<sup>k</sup>, T R Wyatt<sup>p</sup>, R Yaari<sup>z</sup>, A Yeaman<sup>m</sup>, G Yekutieli<sup>z</sup>, M Yurko<sup>r</sup>, W Zeuner<sup>h</sup> and G T Zorn<sup>q</sup>

<sup>a</sup> School of Physics and Space Research, University of Birmingham, Birmingham, B15 2TT, UK

<sup>b</sup> Dipartimento di Fisica dell' Università di Bologna and INFN, Bologna, 40126, Italy

<sup>c</sup> Physikalisches Institut, Universität Bonn, D-5300 Bonn 1, Germany

<sup>d</sup> Department of Physics, University of California, Riverside, California 92521, USA

<sup>e</sup> Cavendish Laboratory, Cambridge, CB3 0HE, UK

<sup>f</sup> Carleton University, Department of Physics, Colonel By Drive, Ottawa, Ontario K1S 5B6, Canada

<sup>g</sup> Centre for Research in Particle Physics, Carleton University, Ottawa, Ontario K1S 5B6, Canada

<sup>h</sup> CERN, European Organisation for Particle Physics, 1211 Geneva 23, Switzerland

<sup>l</sup> Enrico Fermi Institute and Department of Physics, University of Chicago, Chicago, Illinois 60637, USA

<sup>j</sup> Fakultät für Physik, Albert Ludwigs Universität, D-7800 Freiburg, Germany

<sup>k</sup> Physikalisches Institut, Universität Heidelberg, Heidelberg, Germany

<sup>ℓ</sup> Indiana University, Department of Physics, Swain Hall West 117, Bloomington, Indiana 47405, USA

<sup>m</sup> Queen Mary and Westfield College, University of London, London, E1 4NS, UK

<sup>n</sup> Birkbeck College, London, WC1E 7HV, UK

<sup>o</sup> University College London, London, WC1E 6BT, UK

<sup>p</sup> Department of Physics, Schuster Laboratory, The University, Manchester, M13 9PL, UK

<sup>q</sup> Department of Physics, University of Maryland, College Park, Maryland 20742, USA

<sup>r</sup> Laboratoire de Physique Nucleaire, Université de Montreal, Montreal, Quebec H3C 3J7, Canada

<sup>s</sup> University of Oregon, Department of Physics, Eugene, Oregon 97403, USA

<sup>t</sup> Rutherford Appleton Laboratory, Chilton, Didcot, Oxfordshire, OX11 0QX, UK

<sup>u</sup> DAPNIA/SPP, Saclay, F-91191 Gif-sur-Yvette, France

<sup>v</sup> Department of Physics, Technion-Israel Institute of Technology, Haifa 32000, Israel

<sup>w</sup> Department of Physics and Astronomy, Tel Aviv University, Tel Aviv 69978, Israel

<sup>x</sup> International Centre for Elementary Particle Physics and Department of Physics, University of Tokyo, Tokyo 113, Japan

and Kobe University, Kobe 657, Japan

<sup>y</sup> Brunel University, Uxbridge, Middlesex, UB8 3PH, UK

<sup>z</sup> Nuclear Physics Department, Weizmann Institute of Science, Rehovot 76100, Israel

<sup>aa</sup> Universität Hamburg/DESY, II Inst für Experimental Physik, D-2000 Hamburg 52, Germany

<sup>ab</sup> University of Victoria, Department of Physics, P O Box 3055 Victoria, BC V8W 3P6, Canada

<sup>ac</sup> University of British Columbia, Department of Physics, Vancouver, BC V6T 1Z1, Canada

<sup>ad</sup> University of Alberta, Department of Physics, Edmonton, Alberta T6G 2N5, Canada

<sup>ae</sup> Duke University, Department of Physics, Durham, North Carolina 27708-0305, USA

Received 23 June 1993

Editor K. Winter

The lifetime of the  $B_s^0$  meson has been measured with the OPAL detector at LEP. A sample of  $B_s^0$  ( $\bar{B}_s^0$ ) decays has been obtained using  $D_s^- \ell^+$  (and charge conjugate, where  $\ell$  denotes a lepton) combinations, where the  $D_s^-$  was reconstructed in either the  $\phi\pi^-$  or  $K^{*0}K^-$  channel. The decay lengths of  $D_s^- \ell^+$  combinations were measured using vertex reconstruction. Proper decay times were obtained by combining these decay lengths with an estimate of the relativistic boost of the  $B_s^0$  and were used in a maximum likelihood fit for the mean  $B_s^0$  lifetime. From approximately 22  $D_s^- \ell^+$  combinations attributed to  $B_s^0$  decays (after background subtraction) in 1.26 million hadronic  $Z^0$  events recorded between 1990 and 1992, we have measured  $\tau_{B_s} = 1.13_{-0.26}^{+0.35}(\text{stat}) \pm 0.09(\text{sys})$  ps.

## 1. Introduction

The lifetimes of b hadrons are related to both the strength of the b quark coupling to c and u quarks and by the dynamics of b hadron decay. In the spectator model, the light quarks in b hadrons play no role in the decay of the b quark, leading to the prediction that the lifetimes of all b hadrons are equal to the lifetime of the b quark. The prediction of the same model for charmed hadrons is incorrect since the measured  $D^+$  lifetime is approximately 2.5 times the  $D^0$  lifetime [1]. The larger mass of the b quark suggests that b hadron decays should follow more closely the predictions of the spectator model. Although more sophisticated models [2] predict b meson lifetime differences of the order of 10% or less, b baryon lifetimes could differ from mesons by as much as 15–20%. The observation of deviations of much greater magnitude would be very difficult to accommodate in existing models.

In this letter we present a measurement of the lifetime of the  $B_s^0$  meson. The semileptonic decay  $B_s^0 \rightarrow D_s^- \ell^+ \nu X$  is used to tag  $B_s^0$  decays. The proper decay time is determined on an event by event basis using measured decay lengths and estimates of the  $B_s^0$  energy. The following sections describe the OPAL detector, the selection of  $B_s^0$  candidates, the vertex topology of the events, the determination of the  $B_s^0$  decay length, the estimation of the  $B_s^0$  energy, the lifetime fit, the results, and the systematic errors. Charge conjugation is implied throughout this letter.

## 2. The OPAL detector and data sample

The OPAL detector is described in ref. [3]. The portion of the central tracking system common to all data sets comprises a precision vertex drift chamber and a large volume jet chamber surrounded by a set of chambers to measure the z-coordinate<sup>#1</sup>. The central tracking chambers are contained in a four bar pressure vessel immersed in a solenoidal magnetic field of 0.435 T. The impact parameter resolution in the x-y plane achieved for 45 GeV/c muon pair events is  $36 \mu\text{m}$  for tracks in the barrel with 12 vertex chamber hits, and the momentum resolution is approximately  $(\sigma_{p_{xy}}/p_{xy})^2 = (0.02)^2 + (0.0015 p_{xy})^2$ , where  $p_{xy}$  is the transverse momentum in GeV/c. The jet chamber also provides up to 159 samples of the ionization energy loss,  $dE/dx$ , for particle identification with a resolution of 3–4% over a wide range of momenta up to 20 GeV/c. Outside the coil are a time-of-flight scintillator array and a lead glass electromagnetic calorimeter with presampler, followed by a hadron calorimeter consisting of the instrumented return yoke of the magnet, and several layers of muon chambers.

A 1.4 mm thick carbon fiber beam pipe of 7.8 cm radius was in place for the 1990 LEP run. For the 1991 run a high precision silicon microvertex detector [4] surrounding a 1.1 mm thick, 5.3 cm radius beryllium-composite beam pipe was placed inside a new 2.2 mm thick, 8.0 cm radius carbon fiber pipe. The silicon detector was operational for 73% of the data collected in 1991, and all of the data collected in 1992, and provides two layers of silicon strip readout in the x-y plane. The polar angle acceptance is  $|\cos\theta| \leq 0.82$  (0.76) for the inner (outer) layer,

<sup>1</sup> Also at TRIUMF, Vancouver, V6T 2A3, Canada

<sup>2</sup> And IPP, University of Victoria, Department of Physics, P O Box 3055, Victoria, BC V8W 3P6, Canada

<sup>3</sup> Also at Shinshu University, Matsumoto 390, Japan

<sup>#1</sup> The coordinate system is defined so the z-axis follows the electron beam direction and the x-y plane is perpendicular to it with the x-axis lying horizontally. The polar angle  $\theta$  is defined relative to the +z-axis, and the azimuthal angle  $\phi$  is defined relative to the +x-axis.

and the impact parameter resolution in the  $x$ - $y$  plane achieved for 45 GeV/ $c$  muon pairs is 18  $\mu\text{m}$  for tracks with associated hits in both layers of the silicon microvertex detector

Further information on the performance of the tracking and  $dE/dx$  measurements can be found in refs [4-6]

The average intersection point of the electron and positron bunches, or beam spot, is measured using charged tracks in the OPAL data [7] with a technique that follows any significant shifts in the position during a LEP fill. The precision on the coordinates of the centroid is better than 10  $\mu\text{m}$ . The intrinsic width of the beam in the vertical direction is taken to be 8  $\mu\text{m}$ , from considerations of LEP beam optics. The width in the horizontal direction, which is measured directly, is between 100  $\mu\text{m}$  and 160  $\mu\text{m}$ , depending on the LEP optics

### 3. Event selection

The data collected during the 1990-1992 LEP running periods are used in this analysis. The OPAL detector recorded 7  $\text{pb}^{-1}$  integrated luminosity in 1990, 14  $\text{pb}^{-1}$  in 1991, and 25  $\text{pb}^{-1}$  in 1992. After standard hadronic selection [8] and detector performance requirements, a sample of 1.26 million events is selected. The selection of the semileptonic  $B_s^0$  events follows closely that of ref [9]. The identification of hadron species in this analysis relies on ionization energy loss ( $dE/dx$ ) measurements [6] in the OPAL jet chamber in the region  $|\cos\theta| < 0.94$ . Only particles with more than 20  $dE/dx$  samples are identified. Two levels of identification are used, which are defined as follows

(i) A charged track is considered to be *consistent* with a specific particle type if its  $dE/dx$  value is within three standard deviations of the expected  $dE/dx$  for that particle hypothesis

(ii) The more stringent requirement of *positive identification* of a kaon requires that a particle have a  $dE/dx$  value within two standard deviations of the expected  $dE/dx$  value for a kaon, and more than one standard deviation below the  $dE/dx$  expected for a pion

Positive identification is used only for particles with momenta greater than 2 GeV/ $c$ , to avoid the regions

where the  $dE/dx$  values for pions and kaons overlap. The efficiency for particle identification is about 95% for the consistency criterion, and ranges from 74% to 84% for the positive identification of charged kaons in the range of momenta relevant to this analysis. The positive identification criteria for charged kaons rejects about 84% of the charged pions

The electron identification procedure used in this paper is that given in refs [10,11]. Electrons with  $p > 3 \text{ GeV}/c$  in the angular range  $|\cos\theta| < 0.7$  are used in this analysis. The electron identification procedure uses  $dE/dx$ , shower shape information from the electromagnetic calorimeter and presampler, and  $E/p$ , where  $E$  is the energy deposited in the calorimeter around the extrapolated position of the central detector track of momentum  $p$ . Electron candidates which are identified as arising from photon conversions are rejected. The electron identification efficiency is approximately 55%, while the probability of misidentifying a hadron as an electron ranges from 0.003% at  $p \approx 3 \text{ GeV}/c$  to 0.1% at  $p > 10 \text{ GeV}/c$

Muons are identified [10] by associating central detector tracks with track segments in the muon detectors, and requiring a position match in two orthogonal coordinates. The average identification efficiency is approximately 76% for muons with  $p > 3 \text{ GeV}/c$  and  $|\cos\theta| < 0.9$ . The corresponding average probability for a hadron to be misidentified as a prompt muon is estimated to be 0.8%

The  $B_s^0$  is reconstructed in the decay chain  $B_s^0 \rightarrow D_s^- \ell^+ \nu(X)$ , where  $\ell$  is either  $e$  or  $\mu$  and  $D_s^- \rightarrow \phi \pi^-$  with  $\phi \rightarrow K^+ K^-$ , or  $D_s^- \rightarrow K^{*0} K^-$  with  $K^{*0} \rightarrow K^+ \pi^-$ . The requirement demanded in [9] that reconstructed  $D_s^- \rightarrow K^{*0} K^-$  vertices lie on the same side of the beam axis as the  $K^+ K^- \pi^-$  momentum vector is not applied as it may bias the reconstructed  $D_s^- \ell^+$  decay length. Tracks arising from identified secondary vertices due to decays of  $\Lambda$ ,  $K_s^0$  or  $\gamma$  conversions are excluded from  $K^+ K^- \pi^- \ell^+$  combinations. The lepton candidates are required to have  $p_t$ , the transverse momentum with respect to the associated jet direction (calculated with the lepton momentum included) greater than 1.2 GeV/ $c$ . The  $K^+ K^- \pi^-$  combinations are required to carry more than 15% of the beam energy and the invariant mass of the  $K^+ K^- \pi^- \ell^+$  must lie between 3.2 and 5.5 GeV/ $c^2$  in order to suppress the combinatorial background. All charged kaons have to pass the kaon consistency

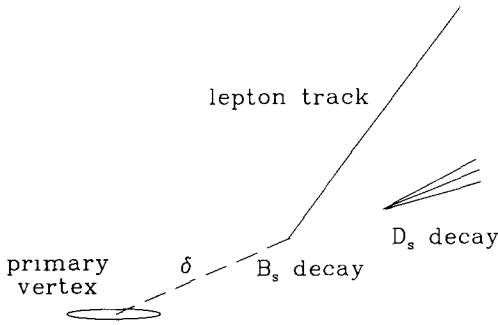


Fig 1 Decay topology for  $B_s^0 \rightarrow D_s^- \ell^+ \nu$ , where  $\delta$  is the measured  $B_s^0$  decay length

For the  $D_s^- \rightarrow K^+ \pi^-$  mode, the invariant mass of the  $K^+ \pi^-$  must lie between  $0.845 \text{ GeV}/c^2$  and  $0.945 \text{ GeV}/c^2$ , and the  $K^-$  must be positively identified to avoid possible confusion with the decay  $D^- \rightarrow K^+ \pi^-$  where it is possible to misidentify the  $\pi^-$  as a  $K^-$ . For the  $D_s^- \rightarrow \phi \pi^-$  mode, the invariant mass of the  $K^+ K^-$  must lie between  $1.005 \text{ GeV}/c^2$  and  $1.035 \text{ GeV}/c^2$ . The cosine of the opening angle between the lepton candidate and the  $K^+ K^- \pi^-$  momentum direction is required to be greater than 0.6 to reduce the number of combinations of leptons and  $D_s$  from different  $b$  hadrons in the same event.

Additional criteria are used to select combinations suitable for precise decay length measurements. The semileptonic decay sequence of  $B_s^0$  leads to two distinct vertices as illustrated in fig 1: the intersection of the lepton and the  $D_s^-$  forms the first decay vertex, and the decay of the  $D_s^-$  forms the second. We first attempt to fit a vertex in the  $x$ - $y$  plane from the decay products of the  $D_s^-$  candidate, using the  $\pi^-$ ,  $K^+$  and  $K^-$  tracks from either the  $\phi \pi^-$  or  $K^+ K^- \pi^-$  channel. The reconstructed  $D_s^-$  momentum is then extrapolated to its intersection with the lepton candidate in the  $x$ - $y$  plane. The two resulting lengths<sup>#2</sup>, from the average beam spot to the  $D_s^- \ell^+$  intersection ( $\delta$  in fig 1), and from the  $D_s^- \ell^+$  intersection to the  $D_s^-$  decay point, are converted into three dimensions using the reconstructed  $\theta$  angles of the  $D_s^- \ell^+$  system, and of the  $D_s^-$ , respectively. The use of the  $D_s^- \ell^+$  momentum vector

<sup>#2</sup> The decay lengths are signed by the cosine of the angle between the position vector of the decay vertex (relative to its assumed production point), and the combined momentum vector of the measured decay particles.

as an estimator for the  $\theta$  of the decaying  $B_s^0$  has been studied with Monte Carlo samples. While the presence of undetected particles in the decay (e.g. the neutrino) and detector resolution produce a smearing in  $\theta$ , the bias due to this approximation is found to be negligible. The average  $B_s^0$  decay length,  $L$ , is about 0.2 cm, while the measurement uncertainty,  $\sigma_L$ , is about  $300 \mu\text{m}$ , and includes contributions from the tracking errors and the uncertainty in the position and intrinsic spread in the beam spot. The  $D_s^-$  decay length (about 0.1 cm) and the  $\chi^2$  of the  $D_s^-$  decay vertex fit are also used to reject background combinations and mismeasurements. In particular, we require

- $|ct_D| < 0.08 \text{ cm}$ ,
- $t_D/\sigma(t_D) > -1.5$ ,
- $\chi_D^2 < 10$ ,

where  $t_D$  is the calculated proper  $D_s^-$  decay time, and  $\chi_D^2$  is the  $\chi^2$  of the  $D_s^-$  vertex fit in the  $x$ - $y$  plane. The projected decay length of the  $D_s^- \ell^+$  combination is determined from a fit where the assumed direction of the  $B_s^0$  in the  $x$ - $y$  plane is constrained to be that of the  $D_s^- \ell^+$  momentum vector.

Further requirements are placed on the quality of the tracks forming the  $D_s^- \ell^+$  candidates to reduce the contamination from poorly reconstructed tracks and pattern recognition mistakes. We require that the lepton candidate and at least 2 of the 3 particles forming the  $D_s^-$  candidate have at least one silicon vertex detector hit, or a majority of "first hits" in the vertex drift chamber<sup>#3</sup>. In order to reduce the contamination from poorly reconstructed events, only those events with measured  $B_s^0$  decay lengths in the range  $-1.0 \text{ cm} < L < 2.0 \text{ cm}$ , and having decay length errors  $\sigma_L < 0.6 \text{ cm}$ , are selected.

The  $K^+ K^- \pi^-$  invariant mass distribution for "right sign" ( $K^+ K^- \pi^- \ell^+$ ) candidates is shown in fig 2, where the  $\phi \pi^-$  and  $K^+ K^-$  contributions have been summed. The dashed-line histogram shows the "wrong sign" ( $K^+ K^- \pi^- \ell^-$ ) combinations. A likelihood fit to a Gaussian signal on a linear background yields a fitted  $D_s^-$  mass of  $1.959 \pm 0.004 \text{ GeV}/c^2$ , and a width of  $0.018 \pm 0.003 \text{ GeV}/c^2$ . The fitted background fraction is  $0.33 \pm 0.05$ , for the interval  $1.915 < m_{KK\pi} < 2.003 \text{ GeV}/c^2$ . The  $D^- \rightarrow \phi \pi^-$  contribution (the peak at  $m_{KK\pi} = 1.86 \text{ GeV}/c^2$ ) is

<sup>#3</sup> The "first hit" on a particular wire is that with the shortest measured drift time.

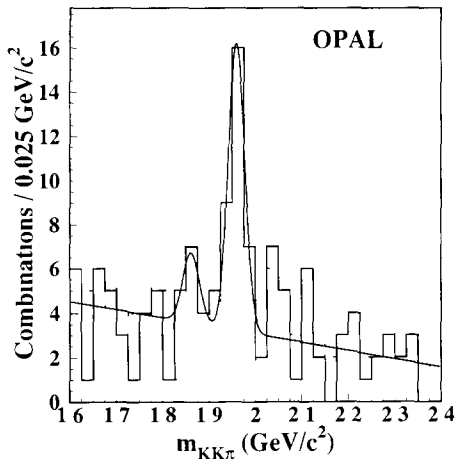


Fig 2 The  $K^+K^-\pi^-$  invariant mass distribution is shown for  $K^+K^-\pi^-\ell^+$  combinations (solid histogram) and  $K^+K^-\pi^-\ell^-$  combinations (dashed histogram) The fitted curve is described in the text

Table 1  
Numbers of events in the signal and sideband regions The masses are in  $\text{GeV}/c^2$

$D_s\ell$ combination	$K^+K^-\pi^-$ mass interval	No of events
right sign	1 915–2 003	33
wrong sign	1 915–2 003	8
right sign	2 050–2 200	17
wrong sign	2 050–2 200	23
total signal events		33
total sideband events		48

fitted to avoid biasing the background estimate, but the contamination from  $D^- \rightarrow \phi\pi^-$  decays in the  $D_s^-$  signal region is negligible. No peak is observed at the  $D_s^-$  mass in the wrong sign combinations.

Table 1 gives the number of events used in the lifetime fit. We define right sign combinations with  $1\,915 < m_{KK\pi} < 2\,003 \text{ GeV}/c^2$  as “signal” events. The expected background in the signal region, based on the fit, is 10.9 events. The total uncertainty in the background fraction is  $\pm 0.10$ , which comes from combining the uncertainty in the fitted background fraction with the binomial error on the expected fraction of background events. The events referred to as “sideband” events come from three categories – wrong sign combinations in the signal region, and both right and

wrong sign combinations in the high-mass region with  $2\,050 < m_{KK\pi} < 2\,200 \text{ GeV}/c^2$ . The decay time distribution of the sideband sample is taken as an estimate of the decay time distribution of the combinatorial background in the signal region. The mass region below the  $D_s^-$  is not used to avoid events which come from partially reconstructed charm decays. The decay time distributions of these signal and sideband samples are used in the maximum likelihood fit for the  $B_s^0$  lifetime.

#### 4. The lifetime fit

##### 4.1 Estimation of the relativistic boost

The measured decay length ( $L_t$ ) for each  $B_s^0$  must be converted into a proper decay time ( $t_i$ ) by correcting for the relativistic boost of the  $B_s^0$  meson via

$$t_i = \frac{L_t}{\beta_i \gamma_i c}, \quad (1)$$

where  $\beta_i \gamma_i$  is the relativistic boost of the  $B_s^0$ . Since the  $B_s^0$  is only partially reconstructed it is necessary to make an estimate of the conversion factor  $1/\beta\gamma$ . An unbiased, event-by-event estimate is made using the  $B_s^0$  mass ( $m_{B_s}$ )<sup>#4</sup>, and the invariant mass ( $m_{D\ell}$ ) and energy ( $E_{D\ell}$ ) reconstructed from the momenta of the four charged tracks forming the  $D_s\ell$  combination. Assuming that the neutrino is the only missing particle, then

$$f(E_{D\ell}, m_{D\ell}^2) = \frac{\Delta}{m_{B_s} E_{D\ell}} \left( \ln \frac{\Sigma + \beta\Delta}{\Sigma - \beta\Delta} \right)^{-1},$$

with  $\Delta \equiv m_{B_s}^2 - m_{D\ell}^2$ ,  $\Sigma \equiv m_{B_s}^2 + m_{D\ell}^2$ , (2)

provides an unbiased estimate of the true conversion factor,  $1/\beta\gamma$ . The root mean square uncertainty of this estimate is

$$\frac{\sigma_f}{f} = \sqrt{\frac{4\beta^2\Delta^2}{\Sigma^2 - \beta^2\Delta^2} \left( \ln \frac{\Sigma + \beta\Delta}{\Sigma - \beta\Delta} \right)^{-2} - 1} \quad (3)$$

Eqs (2) and (3) are both analytical derivations, using exact decay kinematics.

<sup>#4</sup> We use  $m_{B_s} = 5.367 \text{ GeV}/c^2$  in the calculation of  $f(E_{D\ell}, m_{D\ell}^2)$  [12].

Uncertainties due to the presence of unreconstructed particles other than the neutrino are discussed in section 6

#### 4.2 Maximum likelihood fit

The  $B_s^0$  decay time distribution is taken to be an exponential distribution convoluted with a Gaussian resolution function whose width is determined by the uncertainty in the decay time. The likelihood of measuring the decay time  $t_i$  from a parent distribution of lifetime  $\tau_0$  is

$$\begin{aligned} \mathcal{L}_i^B(\tau_0 | t_i, \sigma_i) &= \frac{1}{\tau_0 \sigma_i \sqrt{2\pi}} \\ &\times \int_0^\infty \exp(-t'/\tau_0) \exp\left(-\frac{(t' - t_i)^2}{2\sigma_i^2}\right) dt' \\ &\equiv G(t_i, \sigma_i) \otimes E(\tau_0), \end{aligned} \quad (4)$$

where  $G(t_i, \sigma_i)$  is a Gaussian of width  $\sigma_i$  centered at a mean value of  $t_i$  and  $E(\tau_0)$  is an exponential of mean lifetime  $\tau_0$ . The uncertainty,  $\sigma_i$ , is given by

$$\sigma_i(s) = \frac{L_i}{\beta_i \gamma_i c} \left[ \left( \frac{s \sigma_{L_i}}{L_i} \right)^2 + \left( \frac{\sigma_{f_i}}{f_i} \right)^2 \right]^{1/2}, \quad (5)$$

where the scale factor  $s$  is introduced to allow the fitted lifetime to be independent of a systematic misestimation<sup>#5</sup> of the decay length errors.

The fit must also account for the background combinations present in the  $D_s \ell$  sample. The functional form used to parametrize the background<sup>#6</sup> is a combination of two exponentials, one with a positive lifetime, and the other with a negative lifetime, both convoluted with a Gaussian

$$\begin{aligned} \mathcal{L}_i^{\text{bg}}(\tau^+, \tau^-, f^+ | t_i, \sigma_i) \\ \equiv [f^+ E(\tau^+) + (1 - f^+) E(-\tau^-)] \otimes G(t_i, \sigma_i), \end{aligned} \quad (6)$$

where by definition,  $\tau^-$  and  $\tau^+$  are non-negative, and  $f^+$  is the fraction of the background with lifetime  $\tau^+$

<sup>#5</sup> This is partially due to the imprecise direction constraint used in the decay length calculation

<sup>#6</sup> Only the combinatorial background is addressed here. The changes to the fit results which result from potential sources of physics background are very small and are discussed in section 6

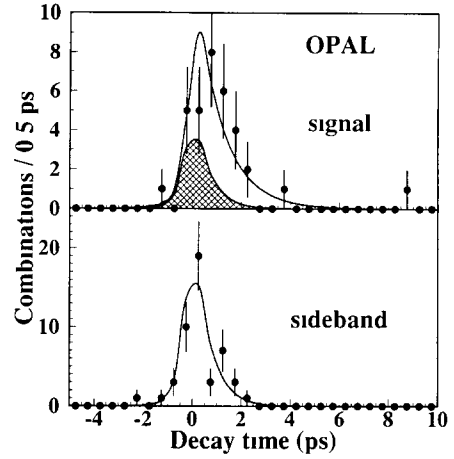


Fig. 3 Top: The decay time distribution of  $K^+K^-\pi^-\ell^+$  combinations from the  $D_s$  mass region. The hatched area represents the background events, scaled from the lower distribution. Bottom: The decay time distribution of  $K^+K^-\pi^-\ell^-$  combinations in the  $D_s$  mass region, and the decay time distribution of  $K^+K^-\pi^-\ell^\pm$  combinations in the high-mass sideband. The curves are described in the text.

The full fit has five free parameters: two ( $\tau_0$  and  $s$ ) which describe the true  $B_s^0$  events, and three ( $\tau^+$ ,  $\tau^-$  and  $f^+$ ) which describe the background events. The background which is present in the signal event sample is taken into account by simultaneously fitting these events with a combination of the likelihood for the  $B_s^0$  decays and that for the background

$$\mathcal{L}_i^{\text{sig}} = (1 - f_{\text{bg}}) \mathcal{L}_i^B + f_{\text{bg}} \mathcal{L}_i^{\text{bg}}, \quad (7)$$

where the background level,  $f_{\text{bg}}$ , is fixed to the fraction previously determined. The sideband event sample is assumed to have the same decay time properties as the background in the signal event sample, and is fitted with the background function only.

A normalization factor for the probability function, calculated for each event, accounts for the reduced range of the decay time in the convolution integral. This factor is very close to unity for the decay length window used in this analysis.

The decay time distributions of the signal events and the sideband events are shown separately in fig. 3. The result of the fit for the  $B_s^0$  lifetime is

$$\tau_{B_s} = 1.13_{-0.26}^{+0.35} \text{ ps}$$

The curves in fig 3 represent the sum of the decay time probability distributions for each event. The figures indicate that the fitted functional forms provide a good description of the data for both signal and background. However, it should be noted that the fit is performed to the unbinned data. The hatched area in the top part of fig 3 is the contribution attributed to background combinations alone.

## 5. Consistency checks

The selection and fitting procedure is verified using a Monte Carlo simulation. A total of 20 000 simulated  $Z^0 \rightarrow b\bar{b} \rightarrow B_s^0 X$ ,  $B_s^0 \rightarrow D_s^- \ell^+ \nu X$  events generated with the JETSET 7.3 parton shower Monte Carlo generator [13] are used. The Peterson fragmentation function with  $\epsilon_b = 0.0035$  is used for  $b$  quarks, the remaining quarks are hadronized according to the LUND symmetric fragmentation function tuned to describe the inclusive distributions of hadronic  $Z^0$  decays [14]. All of the events are generated with a mean  $B_s^0$  lifetime of 1.40 ps and passed through the full OPAL detector simulation [15]. The Monte Carlo sample is processed by the same reconstruction software and selection procedure as is used on the data. The decay lengths of events which passed all selection cuts are used as input to the lifetime fit, assuming there is no background. No evidence of a systematic bias of the measured lifetime is observed in either the selection or reconstruction processes: the generated and fitted lifetimes differ by  $0.01 \pm 0.04$  ps.

As a cross check of the vertex reconstruction and decay length fitting techniques, the analysis method is also applied to a sample of  $D^{*-} \ell^+$  events selected from the OPAL data using, where possible, similar kinematic requirements as for the  $D_s \ell$  sample. We fit the  $\pi$  from the  $D^{*-} \rightarrow \bar{D}^0 \pi^-$  transition and the  $K^+ \pi^-$  from the  $\bar{D}^0$  decay to a common vertex<sup>#7</sup>, then find the intersection of the reconstructed  $\bar{D}^0$  with the lepton track. The fitted lifetime for this sample should be close to the  $B^0$  and  $B^+$  meson lifetimes [16] extracted from a similar sample, but analyzed using substantially different techniques. The fitted result obtained from a sample of about 70 events using data taken af-

ter the silicon microvertex detector was commissioned agrees well with both the  $D^{*-} \ell^+$  lifetimes quoted in [16] and the average  $b$  hadron lifetime [17]. In addition, the fitted decay length error scale factor is consistent with that found for the  $B_s^0$  sample.

The decay length determination constrains the direction in the  $x$ - $y$  plane to be that of the  $D_s \ell$  combination in the calculation of the apparent  $B_s^0$  flight length. Repeating the analysis with no direction constraint, using the distance between the beam spot and the reconstructed  $D_s \ell$  vertex in the  $x$ - $y$  plane divided by the sine of the  $\theta$  angle of the reconstructed  $D_s \ell$  momentum vector, yields an identical result to the direction-constrained fit, but with a slightly larger statistical uncertainty.

The standard fit uses the  $K^+ K^- \pi^- \ell^-$  combinations in the  $D_s$  mass region and the high mass  $K^+ K^- \pi^-$  combinations for the sideband decay time distribution. To test the validity of using these events to determine the background parametrization, a fit is done using only the  $K^+ K^- \pi^- \ell^-$  combinations in the  $D_s$  mass region, no significant difference is observed in the measured lifetime.

Removing the  $-1.0$  cm to  $2.0$  cm decay length window cut also produces no significant change in the measured  $B_s^0$  lifetime.

## 6. Evaluation of systematic errors

Systematic errors from the following sources have been studied:

- Background fraction, source, and parametrization,
- Possible bias of the selection/fitting procedure,
- Estimation of the relativistic boost of the  $B_s^0$  meson,
- The assumed position and size of the beam spot,
- Uncertainties in tracking errors.

The summary of these systematic errors appears in table 2 and their determination is discussed below.

The fraction of the  $D_s^- \ell^+$  candidates in the signal sample coming from combinatorial background has been estimated to be  $33 \pm 10\%$ . Changing the background fraction assumed in the fit by one standard deviation changes  $\tau_B$  by  $0.07$  ps. The fitted lifetime is insensitive to the particular background parametrization, an alternative parametrization with a positive lifetime exponential and a delta function at zero lifetime changes the fitted lifetime by  $0.01$  ps. The back-

<sup>#7</sup> The kinematics of the  $D^{*-} \rightarrow \bar{D}^0 \pi^-$  transition cause the transition  $\pi^-$  to follow closely the  $\bar{D}^0$  flight direction.



Table 2  
Summary of systematic errors on  $\tau_{B_s}$

Source	$\sigma(\tau_{B_s})$ (ps)
background	$\pm 0.07$
possible bias of method	$\pm 0.03$
uncertainty in boost	$\pm 0.04$
beam spot	$\pm 0.01$
alignment errors	$\pm 0.02$
quadrature sum	$\pm 0.09$

grounds in the  $B_s^0 \rightarrow D_s^- \ell^+ \nu$  sample which involve real  $D_s^- \ell^+$  combinations from  $B_{u,d}$  decays have been estimated using Monte Carlo simulations of the processes  $B_{u,d} \rightarrow D_s^- K \ell^+ \nu X$  and  $B_{u,d} \rightarrow D_s^+ \bar{D} X$ ,  $\bar{D} \rightarrow \ell^- X$ , with the generated  $B_u$  and  $B_d$  lifetimes set to 1.4 ps. The first of these sources is expected to contribute less than 1 event to the  $D_s^- \ell^+$  sample, and the second is expected to be completely negligible. The effect of these backgrounds on the fitted  $B_s^0$  lifetime is estimated by introducing a small component with a lifetime fixed at 1.4 ps into the fit. Based on a contamination of 1 event from  $B_{u,d} \rightarrow D_s^- K \ell^+ \nu X$ , we estimate the uncertainty due to this source to be 0.01 ps, and combine this with the variations observed upon changing the parametrization and level of the background to assign a systematic error of 0.07 ps due to uncertainties in the background.

The tests performed on the Monte Carlo samples described in the previous section are consistent with the fit being bias-free. For example, the ratio of the fitted lifetime to the generated lifetime is  $1.006 \pm 0.030$ . We take the statistical precision of this ratio as a potential selection and fitting bias and assign a systematic error of 0.03 ps.

The boost estimation is quite insensitive to the  $b$  fragmentation function for  $B_s^0 \rightarrow D_s^- \ell^+ \nu$  decays. The expression in eq. (2) for estimating the relativistic boost of the  $B_s^0$  is, however, inexact for decays with additional particles (e.g.  $B_s^0 \rightarrow D_s^{*-} \ell^+ \nu$ , or  $B_s^0 \rightarrow D_s^- \ell^+ \nu n\pi$ ). Assuming the fraction of decays to high mass states to be similar to that found in  $B^0$  and  $B^+$  decays (about 30%) [18], we find the expected bias in the estimated boost to be less than 1%. The Monte Carlo is used to compare the fitted lifetimes using the exact boost and the estimated boost. The difference between these results is used to assign a

systematic error of 0.04 ps for a possible uncertainty in the boost estimate, which includes the effects of a 0.1 GeV/c<sup>2</sup> uncertainty in the mass of the  $B_s^0$ .

The average intersection point of the LEP beams in OPAL is used as the estimate of the production vertex of the  $B_s^0$  candidates. The mean  $x$  and  $y$  coordinates of the beam spot are known to better than  $10 \mu\text{m}$ , as is the effective  $r.m.s.$  spread of the beam. This spread in the beam spot in  $x$  is measured in the data to be about  $160 \mu\text{m}$  in 1990 data,  $150 \mu\text{m}$  in 1991 data and  $100 \mu\text{m}$  in 1992 data. The effective spread of the beam spot in  $y$  is about  $20 \mu\text{m}$ , and is dominated by the uncertainty in following beam movements, since the intrinsic width due to LEP optics is expected to be less than  $10 \mu\text{m}$ . To test the sensitivity of  $\tau_{B_s}$  to the assumed position and size of the beam spot, the coordinates of the beam spot are shifted by  $\pm 25 \mu\text{m}$ , and the spreads changed by  $\pm 10 \mu\text{m}$ . The largest observed variation in  $\tau_{B_s}$  is 0.01 ps, which we assign as a systematic error.

The effect of alignment and calibration uncertainties on the result is not studied directly, but is estimated from a detailed study of 3-prong  $\tau$  decays [7], where the uncertainty in the decay length due to these effects is found to be  $43 \mu\text{m}$ . The average decay lengths of taus from  $Z^0$  decay is approximately the same as the average  $B_s^0$  decay length in this analysis, and since the uncertainty is not expected to depend on the opening angles between the detected particles, we assign an error of  $43 \mu\text{m}$  to the decay length, which translates into an uncertainty on  $\tau_{B_s}$  of 0.02 ps.

The total systematic error of 0.09 ps is obtained by adding the individual errors in quadrature.

## 7. Conclusion

A sample of approximately 22  $B_s^0 \rightarrow D_s^- \ell^+ \nu (X)$  decays, with  $D_s^- \rightarrow K^+ K^- \pi^-$  through either the  $\phi\pi^-$  or  $K^{*0}K^-$  channels, has been selected from 1.26 million hadronic  $Z^0$  events recorded between 1990 and 1992. The decay lengths of the  $D_s \ell$  combinations were measured and converted into proper decay times using an event by event estimate of the relativistic boost of the  $B_s^0$ . These decay times and their error estimates were used in a maximum likelihood fit to obtain the mean  $B_s^0$  lifetime, taking into account the combina-

torial background underneath the  $D_s^-$  peak. Based on these decays we find

$$\tau_{B_s} = 1.13_{-0.26}^{+0.35}(\text{stat}) \pm 0.09(\text{sys}) \text{ ps}$$

This result can be compared with the OPAL measurements of the average b hadron lifetime [17] ( $1.524 \pm 0.051$  ps), and the  $B^0$  and  $B^+$  lifetimes [16] ( $1.51 \pm 0.27$  ps and  $1.51_{-0.31}^{+0.32}$  ps, respectively)

### Acknowledgement

It is a pleasure to thank the SL Division for the efficient operation of the LEP accelerator, the precise information on the absolute energy, and their continuing close cooperation with our experimental group. In addition to the support staff at our own institutions we are pleased to acknowledge the Department of Energy, USA, National Science Foundation, USA, Texas National Research Laboratory Commission, USA, Science and Engineering Research Council, UK, Natural Sciences and Engineering Research Council, Canada, Fussesfeld Foundation, Israeli Ministry of Energy, Israeli Ministry of Science, Minerva Gesellschaft, Japanese Ministry of Education, Science and Culture (the Monbusho) and a grant under the Monbusho International Science Research Program, German Israeli Bi-national Science Foundation (GIF), Direction des Sciences de la Matière du Commissariat à l'Énergie Atomique, France, Bundesministerium für Forschung und Technologie, FRG, National Research Council of Canada, Canada, A.P. Sloan Foundation and Junta Nacional de Investigação Científica e Tecnológica, Portugal

### References

- [1] Particle Data Group, K. Hikasa et al., Phys. Rev. D 45 (1992) S1
- [2] I.I. Bigi and N.G. Uraltsev, Phys. Lett. B 280 (1992) 271, G. Altarelli and S. Petrarca, Phys. Lett. B 261 (1991) 303, I.I. Bigi, Phys. Lett. B 169 (1986) 101, J.H. Kuhn et al., Heavy flavours at LEP, MPI-PAE/PTh 49/89 (August 1989), contribution by R. Ruckl, p. 59
- [3] OPAL Collab., K. Ahmet et al., Nucl. Instrum. and Meth. A 305 (1991) 275
- [4] P.P. Allport et al., Nucl. Instrum. and Meth. A 324 (1993) 34
- [5] O. Biebel et al., Nucl. Instrum. and Meth. A 323 (1992) 169
- [6] M. Hauschild et al., Nucl. Instrum. and Meth. A 314 (1992) 74
- [7] OPAL Collab., P.D. Acton et al., Measurement of the  $\tau$  lifetime, CERN PPE/93-09, 15 January 1993, to appear in Z Phys
- [8] OPAL Collab., G. Alexander et al., Z Phys. C 52 (1991) 175
- [9] OPAL Collab., P.D. Acton et al., Phys. Lett. B 295 (1992) 357
- [10] OPAL Collab., P.D. Acton et al., Measurement of  $\Gamma_{bb^-}/\Gamma_{\text{had}}$  using leptons, CERN PPE/93-46, 9 March 1993, submitted to Z Phys
- [11] OPAL Collab., P.D. Acton et al., Z Phys. C 55 (1992) 191
- [12] W. Kwong and J.L. Rosner, Phys. Rev. D 44 (1991) 212
- [13] T. Sjostrand, JETSET7.3 Manual, CERN-TH.6488/92, the OPAL parameter optimization is described in OPAL Collab., M.Z. Akrawy et al., Z Phys. C 47 (1990) 503
- [14] OPAL Collab., M.Z. Akrawy et al., Phys. Lett. B 242 (1990) 299
- [15] J. Allison et al., Nucl. Instrum. and Meth. A 317 (1992) 47
- [16] OPAL Collab., P.D. Acton et al., Phys. Lett. B 307 (1993) 247
- [17] OPAL Collab., P.D. Acton et al., Measurement of the average b hadron lifetime in  $Z^0$  decays, CERN PPE/93-92, 4 June 1993, to appear in Z Phys
- [18] CLEO Collab., R. Fulton et al., Phys. Rev. D 43 (1991) 651, ARGUS Collab., H. Albrecht et al., DESY/92-146 (1992)